

# RSC Advances



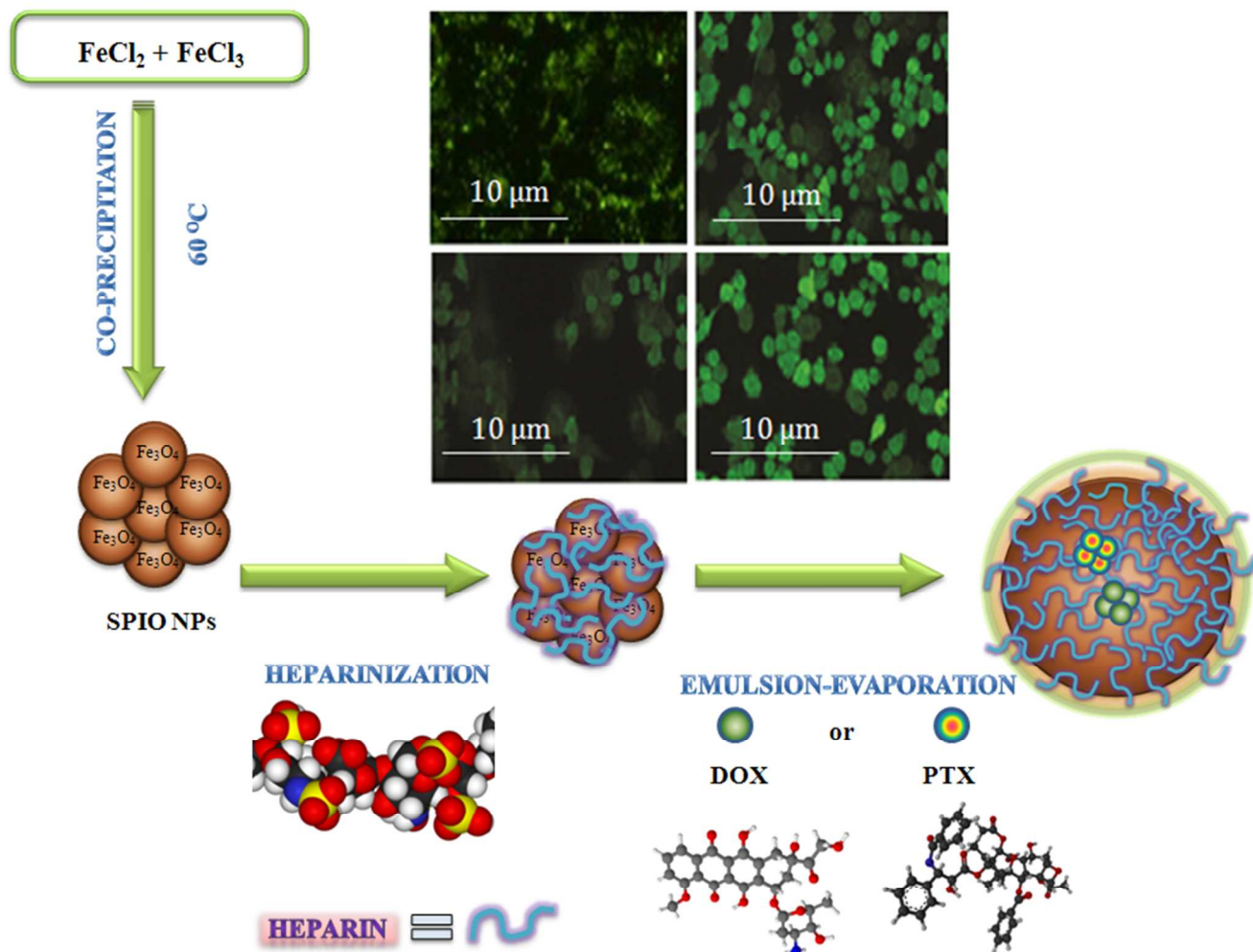
This is an *Accepted Manuscript*, which has been through the Royal Society of Chemistry peer review process and has been accepted for publication.

*Accepted Manuscripts* are published online shortly after acceptance, before technical editing, formatting and proof reading. Using this free service, authors can make their results available to the community, in citable form, before we publish the edited article. This *Accepted Manuscript* will be replaced by the edited, formatted and paginated article as soon as this is available.

You can find more information about *Accepted Manuscripts* in the [Information for Authors](#).

Please note that technical editing may introduce minor changes to the text and/or graphics, which may alter content. The journal's standard [Terms & Conditions](#) and the [Ethical guidelines](#) still apply. In no event shall the Royal Society of Chemistry be held responsible for any errors or omissions in this *Accepted Manuscript* or any consequences arising from the use of any information it contains.

**Novel biodegradable heparin-coated nanocomposite system of anticancer drug  
encapsulation for targeted drug delivery**



### **Highlights**

- HP-SPIO NPs (42 nm) were formulated by co-precipitation technique.
- Doxorubicin and paclitaxel were loaded into the SPIO NP core.
- HP-SPIO NPs had sustained release of DOX (87%) and PTX (75%) at pH 6.0.
- Drug loaded HP-SPIO NPs caused 95, 84%, and 85 and 77% apoptosis in A2780 and OVCAR-3 cells.
- DOX-HP-SPIO NPs and PTX-HP-SPIO NPs caused sharp decrease in bcl-2 and survivin proteins.

# Novel biodegradable heparin-coated nanocomposite system for targeted drug delivery

Amaneh Javid,<sup>a</sup> Shahin Ahmadian,<sup>\*a,b</sup> Ali Akbar Saboury,<sup>a</sup> Seyed Mehdi Kalantar,<sup>c</sup> Saeed Rezaei-Zarchi<sup>d</sup>

<sup>a</sup> *Institute of Biochemistry and Biophysics, University of Tehran, Tehran, Iran*

<sup>b</sup> *Center of Excellence of Nano-Biomedicine, Nano-Science and Nano-Technology Research Center, University of Tehran, Tehran, Iran*

<sup>c</sup> *Research and Clinical Center of Infertility, Shahid Sadoughi University Medical Sciences, Yazd, Iran*

<sup>d</sup> *Department of Biology, Payame Noor University, Yazd, Iran*

\* Corresponding author at: Institute of Biochemistry and Biophysics, University of Tehran, Tehran, Iran. Tel.: +98 21 66956983.

E-mail: [ahmadian@ibb.ut.ac.ir](mailto:ahmadian@ibb.ut.ac.ir) (S. Ahmadian).

15

20

25

**ABSTRACT**

The bare (~10 nm) and heparin (HP)-coated superparamagnetic iron oxide nanoparticles (SPIO NPs; 42 nm) were formulated by co-precipitation technique. The bare and HP-SPIO NPs had saturation magnetization of 50-55 emu/g at 300 K. The anticancer drugs, doxorubicin (DOX) and paclitaxel (PTX), were separately partitioned in the SPIO core to compare their anti-neoplastic effects on the proliferation of A2780 and OVCAR-3 human ovarian cancer cells. Results revealed that the DOX-HP-SPIO NPs (85 nm) and PTX-HP-SPIO NPs (71 nm) showed sustained and pH-sensitive release of DOX (87%) and PTX (75%) at pH 6.0, even for up to two weeks. While, 10 µg/ml DOX-HP-SPIO NPs and PTX-HP-SPIO NP caused 95, 84%, and 85 and 77% apoptosis in A2780 and OVCAR-3 cells, respectively, with a sharp decrease in the level of bcl-2 and survivin proteins and increased expression of proapoptotic proteins, like bax and NF-κB. So, the presently formulated nanocomposite-based drug delivery system was readily internalized into tumor cells and induced a higher apoptosis rate.

µg/ml

**Keywords:** Human ovarian cancer, iron oxide, heparin, drug release, loading efficiency, apoptosis.

15

20

**1. Introduction**

Amongst the broad spectrum of nanoscale materials being investigated for biomedical use, the superparamagnetic iron oxide nanoparticles (SPIO NPs) have created significant interest due to their intrinsic magnetic properties for guided delivery of drugs (Dilnawaz et al., 2010; Kumar et al., 2012). Freeman et al., were the first to introduce the concept of use of magnetism in medicine in the 1970s. Since then, much research has been done in this area, leading to the design of various magnetic particles and vectors. In order to fully exploit the potential of SPIO NPs for image-guided drug delivery upon systemic

administration, they should be biocompatible, stable in the circulation, and the potential for prolonged circulation in the blood stream. This can be circumvented by coating the SPIO NPs with hydrophilic polymers that preferably give them 'stealth' properties. The coatings with hydrophilic polymers were carried out to improve their colloidal stability and also prolong circulation kinetics (Basti et al., 2010; Kim et al., 2009).

5 However, the coated SPIO NPs have limited drug loading capacity and the rapidly dissociation after administration for drug delivery purposes. The main objective of today's leading research is to optimize the properties of these magnetic particles to: provide an increase in magnetic nanoparticle concentration in blood vessels; reduce early clearance from the body; minimize nonspecific cell interactions, thus minimizing side effects; and increase their internalization efficiency within target cells, thus reducing the total dose required (Mahmoudi et al., 2011; Douziech-Eyrolles et al., 2007).

10 The rationale behind the association of drugs with colloidal carriers such as NPs or liposomes is due to the limited success of conventional drug therapy. Systemically administering bolus doses of powerful chemotherapeutics often results in intense side effects due to the action of the drugs on sites other than the intended target sites (Wang et al., 2009). With such nonspecific drug action, the concentration of the drug administered to the patient is a vicious predicament between choosing a near-toxic effective dose and a comfortable ineffective dose (Acharya et al., 2011).

15 Carbohydrate moieties and hydrophilic synthetic polymers are widely utilized for these purposes. Heparin and heparan sulfates are a family of very heterogeneous and highly charged (sulfated and anionic) glycosaminoglycans, which naturally cover the surface of all eukaryotic cells (Kemp, & Linhardt, 2010). These sugars possess various biological activities, which are particularly seen in heparin that is being used as an anticoagulant drug since 1930 (Meng et al., 2010; Villanueva et al., 2009). Heparin is non-cytotoxic, biodegradable, and water-soluble natural polysaccharide, coupled with a variety of biological  
20 activities including anti-coagulation, anti-inflammation, anti-angiogenesis, and anti-tumor cell proliferation, has attracted intense attention. Many heparin-drug conjugates have been developed for cancer chemotherapy as macromolecular prodrugs. These heparin conjugates, containing anticancer agents such as paclitaxel (PTX), exhibited enhanced targeting ability to the tumor and higher therapeutic efficacy compared to free drugs (Kyoung et al., 2004; Sang et al., 2006).

Taking into account the advantage of excellent properties of HP and polymer-drug conjugates, we have successfully  
25 synthesized a HP based SPIO NP drug conjugates, carrying two different anticancer drugs, DOX and PTX, for intra-tumoral drug delivery. The cytotoxicity response of the drug loaded HP-SPIO NPs was determined on the biochemical parameters and survival of human ovarian cancer cell lines of OVCAR-3 and A2780.

## 30 **2. Materials and methods**

### *2.1. Chemicals*

The ovarian cancer cell lines, A2780 (NCBI code, C461) and OVCAR-3 (NCBI code, C430) were purchased from Pasteur Institute, Tehran, Iran. RPMI-1640 medium and all of the additives were purchased from GIBCO Co. (Grand Island, NY, USA). DOX, PTX and heparin were purchased from Sigma-Aldrich Chemical Co. (St. Louis, Missouri, USA). All other chemicals, used, were of the highest purity and biological grade available from the commercial sources.

5

### 2.2. Synthesis of bare and HP-SPIO NPs

Bare SPIO NPs were prepared by co-precipitation technique, with some modification in the previously stated method (Jung et al., 2011; Mohammadi-Samani et al., 2013; Saifuddin & Dinara 2012). Firstly, 5.41 g of  $\text{FeCl}_3 \cdot 6\text{H}_2\text{O}$  (99% purity) and 10 1.99 g  $\text{FeCl}_2 \cdot 4\text{H}_2\text{O}$  (99% purity) were dissolved in 100 ml of distilled water (DW) in a triple-necked flask. The pH of the mixture (100 ml) was maintained at pH 6.9, with slow addition of 25 ml of  $\text{NH}_4\text{OH}$  (25–28%, w/w) while stirring constantly under the protection of dry nitrogen at 60 °C. At this time, the solution color changed from yellow to deep black, indicating the formation of iron oxide particles.

After 1 h of stirring, the prepared SPIO NPs were rinsed with DW and subsequently mixed with UF-HP (5.47 mg/ml) for 15 2 h. The resultant product was then sonicated for 1h, centrifuged at  $10,000 \times g$  for 30 min. and vigorously stirred for 1 h at 90 °C under nitrogen atmosphere.  $M_{\text{ext}}$  was applied for 15-20 sec. to get the aggregates of modified particles. Centrifugation ( $4000 \times g$ ; 10 min.) was carried out to completely separate the particles, remained in the supernatant. The supernatant was concentrated through ultrafiltration system (Model 8200; Amicon Corp., Danvers, MA) using ultrafiltration Amicon YM membrane (100K MWCO, Millipore, Billerica, MA). The resulting HP-SPIO NPs were stored at 4 °C till further use.

20

### 2.3. Drug conjugation to the HP-SPIO NPs

Drug loading onto the HP-SPIO NPs was carried out using oil-in-water single emulsion evaporation method. Three equivalents of triethylamine were added to an aqueous solution, either, of the DOX hydrochloride or PTX (5 mg/ml), and the 25 drug was then extracted to prepare their methylene chloride solutions. The 0.1-10  $\mu\text{g}$  of either of the drugs (10% w/w) were separately dissolved in 1 ml of the organic solvent acetonitrile. The drugs were added drop wise to the HP-SPIO NPs suspension and stirred overnight to allow the partitioning of the drug into SPIO NPs. The unattached drugs were washed with water and separated by centrifuging the suspension at 14000 rpm for 10 min. at 10 °C. A three-time washing was done to remove the unbound drugs. The pellets were lyophilized to get powdered drug loaded HP-SPIO NPs.

30

### 2.4. Loading-efficiency of incorporated drug

The quantification and release kinetics of drug-loading onto the modified nanocomposites was carried out through UV/Visible double-beam spectrophotometer (Hitachi U-2000) at 200-800 nm. Drug incorporation efficiency was observed both as drug loading (% w/w) and drug entrapment (%), by the below-stated equations (1 & 2), respectively.

$$\text{Drug loading } \left(\% \frac{w}{w}\right) = \frac{\text{Mass of drug loaded in NPs}}{\text{Mass of NPs}} \times 100 \quad \dots (1)$$

5

$$\text{Drug entrapment } (\%) = \frac{\text{Mass of drug loaded in NPs}}{\text{Mass of drug used in formulation}} \times 100 \quad \dots (2)$$

### 2.5. Physicochemical properties of drug-loaded HP-SPIO NPs

10

#### a) Microscopic evaluation

Morphological and size evaluation of the bare, HP-modified and drug-loaded NPs was carried out using TEM (H-7600, Hitachi; 200 kV) after negative staining with uranyl acetate solution (1% w/v). The size estimation was based on 25-30 nanoparticles on 3 different images. Surface characterization of bare, HP-coated and HP-coated drug-loaded NPs was carried out using Scanning electron microscopy (SEM).

The AFM topographic images were collected in contact mode using silicon nitride cantilevers (PSIA, Korea, spring constant 0.6 N/m; tip radius <10 nm) using an XE100 (PSIA, Korea) in air. For AFM analysis, the HP-SPIO NPs were diluted with DW and a drop of the diluents was placed on a glass plate and analyzed with AFM equipment.

20

#### b) Magnetization analysis

The magnetization measurements were carried out at room temperature using a vibrating sample magnetometer (VSM, Oxford Instruments, UK), with the magnetic field range of -1 to +1 Tesla (T).

25

#### c) FTIR and XRD analyses

The presence of HP-coating onto the surface of SPIO NPs was studied by wavelength-dependent data of transmittance, obtained for the powdered samples of bare and HP-SPIO NPs, pressed into KBr pellets. The experiment was carried out using

FTIR Spectrophotometer (Model 8300, Shimadzu Corporation, Tokyo, Japan) at 4000 to 400  $\text{cm}^{-1}$ . The crystallographic state of bare and HP-SPIO NPs was determined by XRD (JDX -8030).

d) Dynamic Light Scattering (DLS) and zeta potential evaluation

5

Dynamic light scattering instrument (DLS, MALVERN Zetasizer Nano-ZS) was used for analyzing zeta potential and hydrodynamic diameter measurements, which provided information on the stability of hydrated particles of bare and HP-SPIO NPs in pure water. The samples were diluted in deionized water ( $[\text{Fe}] \sim 2 \times 10^{-3}$  g/l). Each measurement was performed at 25 °C, in triplicate, with a He-Ne laser (4 mW) operating at 633 nm, with the scatter angle fixed at  $173^\circ$ . The polydispersity index (PDI) was used as a measure of broadness of the size distribution. Zeta potential was determined as a function of pH, ranging from 2-12, using 0.1 M  $\text{HNO}_3$  and KOH.

10

*2.6. In vitro drug release profile*

15

Five milligrams of DOX-HP-SPIO NPs and PTX-HP-SPIO NPs were suspended in 10 ml of RPMI medium at different pH conditions (pH 1.5, 6.0 and 7.0) and sonicated to produce a clear solution. The solutions containing bare, HP-coated, DOX-HP-SPIO and PTX-HP-SPIO NPs were placed into dialysis bags (molecular weight cut-off 12,000–14,000 g/mol) containing 35 ml of PBS and incubated in the water bath at 37 °C with gentle shaking at 50 rpm. At predetermined intervals, buffered solutions were collected and replaced with an equivalent volume of fresh PBS. The amount of drug released was determined by HPLC and the drug content was determined spectrophotometrically at 200-800 nm.

20

*2.7. Human ovarian cancer cell culture and in vitro cytotoxicity detection*

The A2780 and OVCAR-3 cells were maintained in RPMI medium, augmented to contain 10% (v/v) FBS, 0.25 IU/ml insulin, 100 mg/ml streptomycin, 100 units/ml penicillin and 0.3 mg/ml glutamine. Cells were cultured in the 96-welled plates for 48 hours, at a density of  $1 \times 10^5$  cells/well, in a humidified atmosphere of 5%  $\text{CO}_2$  in air at 37 °C. The cells were then incubated with bare, HP-coated, DOX-HP-SPIO and PTX-HP-SPIO NPs at a fixed concentration of 10  $\mu\text{g}/\text{ml}$  for 48 h. After the incubation completion, 100  $\mu\text{l}$  of the medium containing 20  $\mu\text{l}$  methylthiazol tetrazolium (MTT) solution was added to each well, and the plates were incubated for an additional 4 h, followed by the addition of 100  $\mu\text{l}$  of MTT solubilization solution containing 10% Triton X-100 + 0.1 N HCl in anhydrous isopropanol to each well. The solution was gently mixed to dissolve the MTT formazan crystals, and the absorbance of each well was measured with a microplate reader at a wavelength of 570 nm. The background absorbance of the wells was measured at 690 nm and subtracted from the results taken from the

30

570 nm experiment. Untreated cells were used as the control. Cell viability was expressed as a percentage of a control that had not been treated with drug-loaded nanoparticles, using the following equation:  $\text{Viability}(\%) = \left(\frac{N_i}{N_c}\right) \times 100 \dots (3)$

Where,  $N_i$  and  $N_c$  are the number of surviving cells in the treatment and control group, respectively.

### 2.8. Apoptotic detection by flowcytometry

A2780 and OVCAR-3 cells were plated at  $5 \times 10^5$  cells per well in 2 ml RPMI-1640 in six-welled plates and incubated for 24 h. The medium was then replaced with 10  $\mu\text{g/ml}$  of each of the bare, HP-coated, DOX-loaded HP-coated and PTX-loaded HP-SPIONs, in separate plates and incubated again for 48 hours. Apoptotic cells were identified with fluorescein isothiocyanate-labeled Annexin V (Annexin V-FITC). Propidium iodide (PI) (BioVision, Mountain View, CA) was used, according to the manufacturer's protocol, to mark the dead cells. All the test materials were diluted with RPMI-1640 medium. The treated cells were harvested, trypsinized, washed with PBS, incubated with Annexin V-FITC and PI for 15 minutes at room temperature in the dark, and analyzed via the FACS-Calibur flowcytometer (Becton, Dickinson & Company, Mountain View, CA) with data acquisition software (CellQuest; Becton, Dickinson and Company).

### 2.9. Immuno-blot analysis and investigation of gene expression

A2780 and OVCAR-3 cells were lysed in a buffer containing 50 mM Tris/HCl (pH 7.4), 150 mM NaCl, 1 mM EDTA, 0.2% (v/v) Nonidet P40 and protease inhibitor cocktail in ice for a period of 10 minutes. Cell debris was pelleted by centrifugation, and the total protein concentration of the soluble extracts was determined by Bradford assay, according to the manufacturer's instructions. Total soluble protein extract (30  $\mu\text{g}$ ) for each sample was resolved by SDS PAGE (12% gels). After electrophoresis, the survivin, Bcl-2, bax and NF- $\kappa$ B proteins were transferred to nitrocellulose, and the blot was blocked for 1 hour at room temperature with a solution of 5% dried milk in PBST (0.1% (v/v) Tween 20 in PBS). The blot was incubated, overnight at 4  $^{\circ}\text{C}$ , with either of the anti-Bcl-2 monoclonal antibody, anti-bax, anti-NF- $\kappa$ B and anti-survivin polyclonal antibodies to evaluate the levels of protein expression. Primary antibodies were detected using an HRP conjugated secondary antibody and enhanced chemiluminescence (ECL) was taken as described by the manufacturer.

25

### 2.10. Statistical analysis

All data were analyzed with SPSS software (version 14.0; SPSS Inc, Chicago, IL). Results were presented as mean  $\pm$  standard deviation (SD). The two-way analysis of variance (ANOVA) and Student's *t*-test were used to compare data from different treatment groups, and differences were considered significant at  $p < 0.05$ .

### 3. Results and discussion

#### 3.1. Characterization of the bare, HP-coated and drug loaded SPIO NPs

5

##### a) TEM and AFM analyses

The nanostructure of bare and HP-SPIO NPs was examined by high resolution TEM, as shown in **Figure 1 (A & B)**. The histograms of the particle size distribution (**Figure 1 C and D**) were obtained by image processing of the TEM micrographs and a subsequent fit to a log-normal distribution function. The estimated mean diameters of the bare and HP-SPIO NPs were 10.12 and 42 nm, respectively (**Figure 1 A-D**). For both samples, a broad distribution of nanoparticle sizes, as well as the agglomerations of iron oxide particles, was observed. This may be caused by polymer adsorption onto the surface of SPIO NPs during synthesis, which prevents the growth of these particles and leads to their better separation. **Figures 1 E and F** demonstrate the atomic force microscopic (AFM) analysis of the bare SPIO NPs and HP-SPIO NPs, which confirm the results of TEM analysis for the present NPs.

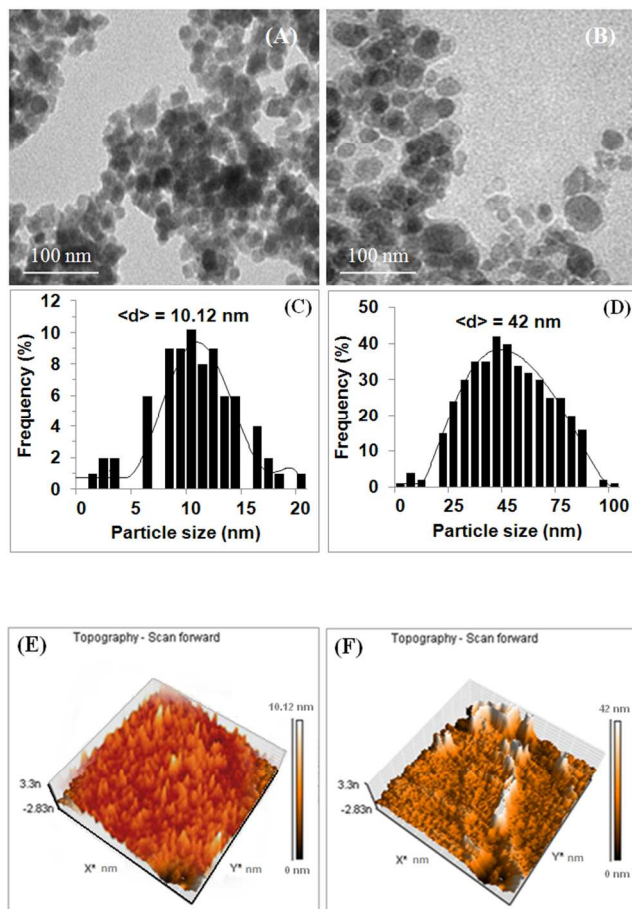


**Figure 1.** TEM micrographs (A and B) and histograms (C and D) of particle size distributions, described by a log-normal distribution function for bare (A and C) and HP-coated (B and D) SPIO-NPs, respectively. The histograms show the average values of 30 measurements. Figures (E) and (F) demonstrate the AFM micrographs of bare SPIO NPs and HP-SPIO NPs, respectively.

5

b) FT-IR analysis

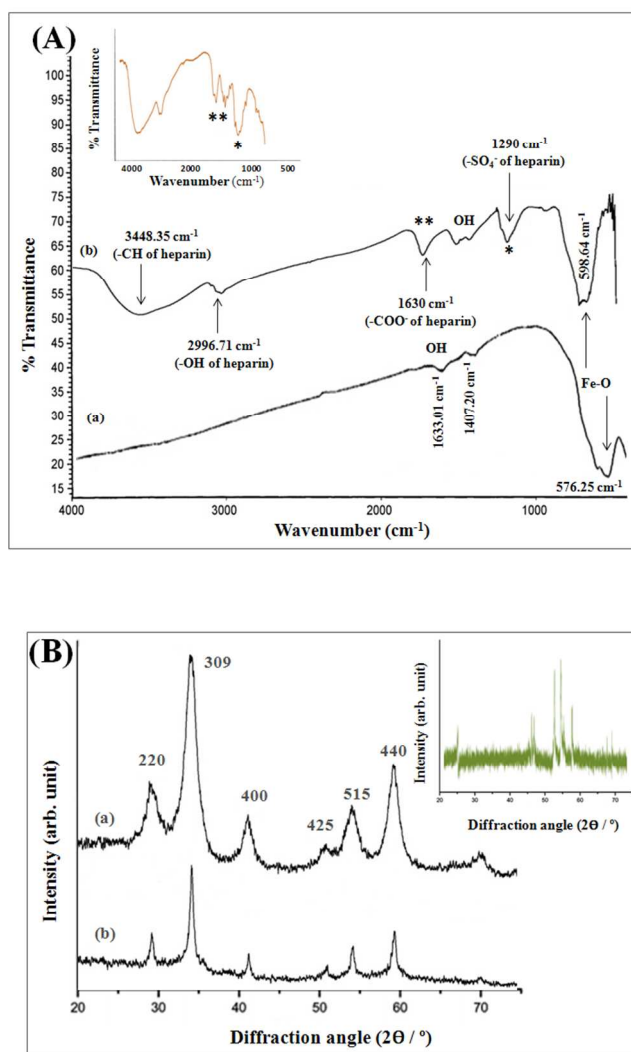
The surface functional groups of the bare and coated NPs were characterized by FT-IR analysis. **Figure 2A** shows the FT-IR spectra of bare and HP-SPIO NPs. Spectrum (a) shows the Fe-O stretching vibration bands at  $576.25\text{ cm}^{-1}$ . While, the peaks of  $1407.20$  and  $1633.01\text{ cm}^{-1}$  represent the stretching vibrations of OH and the bending vibration of the  $\text{H}_2\text{O}$  molecules, respectively. While, the  $1290$  and  $1630\text{ cm}^{-1}$  peaks of the spectrum (b) represent the stretching vibrations of the  $-\text{SO}^{4-}$  and  $-\text{COO}^-$  groups of heparin, respectively; demonstrating that the heparin was successfully coated onto the SPIO NPs. The inset shows the FT-IR spectrum of pure heparin.

15

c) XRD analysis

**Figure 2B** demonstrates the powder XRD analysis of the crystallographic structure and physical properties of the bare and HP-coated NPs. The spectra of the bare and HP-SPIO NPs show identical characteristic diffraction peaks at  $2\theta = 28^\circ$ ,  $33.5^\circ$ ,  $42.0^\circ$ ,  $51.4^\circ$ ,  $54.0^\circ$  and  $58.8^\circ$ , corresponds to the reflection plane indices of (220), (309), (400), (425), (515) and (440), respectively (Liu et al., 2006; Strable et al., 2001). However, no peaks corresponding to  $\gamma\text{-Fe}_2\text{O}_3$  and  $\alpha\text{-Fe}_2\text{O}_3$  like 210, 213 etc. were observed suggesting the purity of SPIO NPs. The XRD pattern of HP-SPIO NPs depicted the same peaks at the same position (**Figure 2B**). This reveals that the surface modification and conjugation of the SPIO NPs to HP did not lead to their phase change. The inset of **Figure 2B** shows the XRD patterns of the pure heparin.

25



5 **Figure 2.** (A) FT-IR spectra of (a) bare and (b) HP-coated SPIO-NPs. The inset represents the FT-IR spectrum of the pure heparin (\* and \*\* represent the positions of  $\text{COO}^-$  and  $\text{SO}_4^-$  bonds of heparin in free and combined state. (B) The X-ray diffraction patterns of (a) bare SPIO-NPs and (b) heparin-coated SPIO-NPs. Peak broadening occurs in coated nanoparticles due to decrease in crystallinity. Inset represents the XRD patterns of the pure heparin.

10 d) Zeta potential and magnetization analysis

**Figure 3A** represents the zeta potential variations under different pH conditions (pH 2.0 - 12.0). The spherical bare and HP-NPs (100%) showed hydrodynamic diameters (~ 10 and 42 nm) with 0.2 PDI. Bare SPIO NPs had about 10, -27 and -45 mV zeta potentials at pH 8.0, 10 and 12, respectively, which can be attributed to the effect of hydrogen bonding taking place with NP moieties at basic pH. While, HP coating onto the NPs changed their potential to highly negative value. This positive to negative shift of potential in bare NPs was recorded at pH 8.5. HP-SPIO NPs showed maximum negative (-34 mV) potential at pH 12, because of the presence of highly negative sulfate groups in the HP molecules. and -30 mV zeta potential. While, positive zeta potential (+28 mV) was recorded for the HP-SPIO NPs, which can be attributed to the hydration of polymer coating, surrounding the magnetite core (Jain et al., 2005).

The Zeta potential is a bulk property, the magnitude of which gives an indication of the potential stability of colloidal system. The large negative or positive zeta potential value in the suspension diminishes the aggregation behavior of particles (Vandana et al., 2009). The high positive-zeta potential formulated HP-SPIO NPs did not change significantly with the increase of HP coating and also after drug loading, describing their colloidal stability in the aqueous solution that could escape the reticuloendothelial system preventing their uptake by macrophages (Sahoo et al., 2003).

The formation of magnetic beads in HP-coated NPs was confirmed by a change in saturation magnetization amounts. According to VSM analysis, the SPIO NPs retained superparamagnetic behavior even after HP coating. **Figure 3B** demonstrates typical hysteresis curves at 10, 150 and 300 K for the optimized HP-SPIO NPs. The hysteresis loop had negligible coercivity at room temperature, and the saturation magnetization ( $M_s$ ) value, at 1.0 T (after subtracting the diamagnetic background), were between 50-55 emu/g at 300 K, which is lower than the bulk value, 90 emu g<sup>-1</sup>. The nanoparticles were not supermagnetic at 10 K. Ideal superparamagnetic materials should have zero coercivity and zero remanence. From the magnetization values, it can be measured that 100% w/w HP-SPIO NPs had in fact only 15% w/w HP coating on their surface.

The inset of **Figure 3B** shows the photographs of HP-SPIO NPs dispersed in solution (left). The application of an external magnetic field ( $M_{ext}$ ) to the container caused the attraction of NPs towards it and their attachment to the wall of the container in close proximity to the magnet and the dispersion became clear (right-side photograph). Removal of  $M_{ext}$  and shaking led to the complete recovery of dispersion, confirming that the prepared HP-SPIO NPs were sensitive to  $M_{ext}$  and showed superparamagnetic property, which shows that the magnetite (Fe<sub>3</sub>O<sub>4</sub>) load in the presently synthesized formulation is quite sufficient to respond to  $M_{ext}$ .

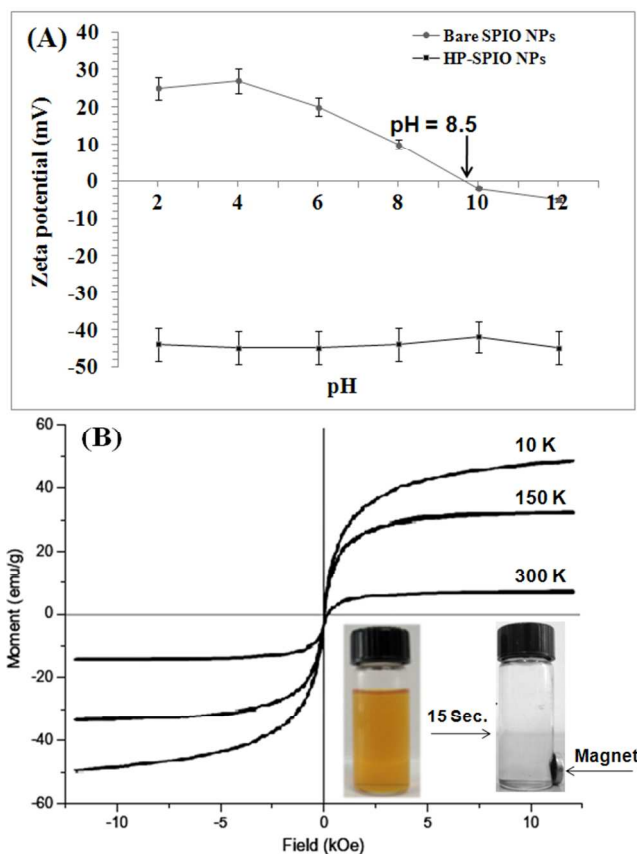


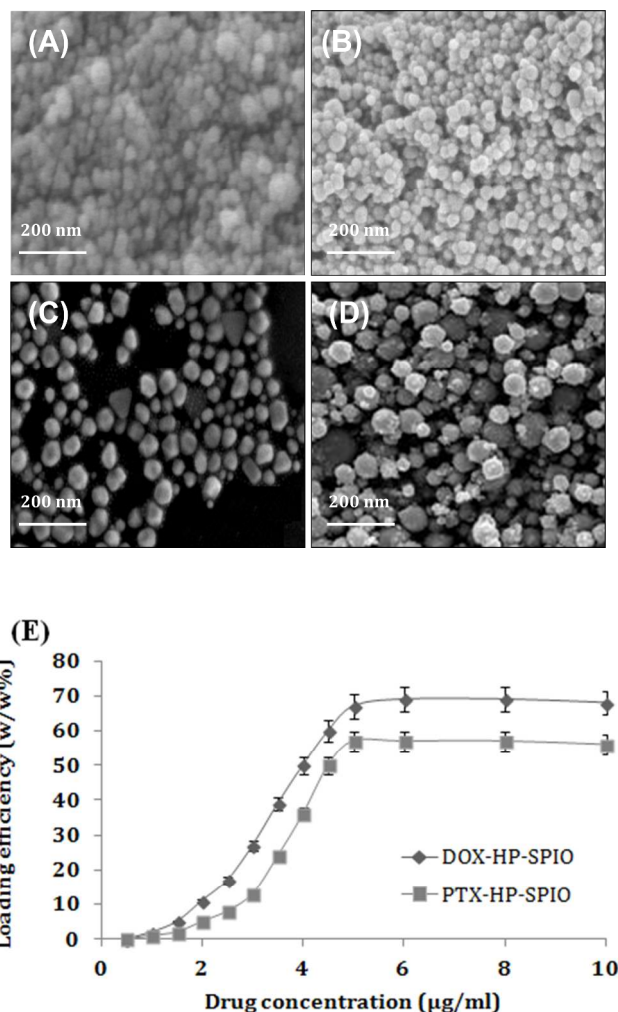
**Figure 3.** (A) Variations of zeta potentials of pure and HP-coated NPs are shown as a function of the pH of surrounding medium. (B) Magnetization curve of the HP-coated SPIO-NPs, as a function of magnetic field, measured at different temperatures (10, 150 and 300 K). Digital photographs of inset show the as-prepared SPIO-NPs in the aqueous suspension (left) and their magnetic separation by applying an  $M_{\text{ext}}$  (right).

### 3.2. Drug loading profile of HP-SPIO NPs

10

Drug loading onto the HP-SPIO NPs was carried out using oil-in-water single emulsion evaporation method. The surface morphology of drug-loaded nanocomposites was evaluated by SEM. **Figure 4** shows the SEM micrographs of the bare (a), HP-SPIO (b), DOX-HP-SPIO (c) and PTX-HP-SPIO NPs (d), respectively. The micrographs revealed that the HP-NPs complex was largely composed of globular structures of various sizes, dispersed throughout the matrix (**Figure 4B**). The mean diameter of the globular structures was estimated to be about 42 nm. While, after drug loading, the dispersed and spherical structures were seen with increased particle size (85 and 71 nm) for the DOX- and PTX-HP-SPIO NPs, respectively (**Figures 4C and D**).

**Figure 4 (E)** shows that 10  $\mu\text{g/ml}$  DOX-HP-SPIO NPs and PTX-HP-SPIO NPs showed 66 and 57% loading efficiencies at the physiological pH.



5

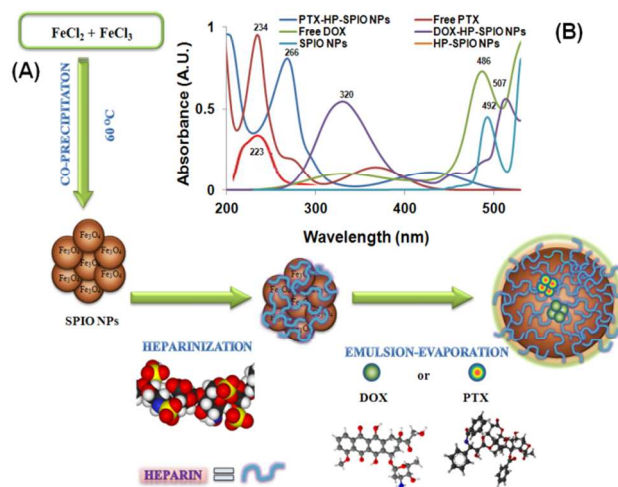
**Figure 4.** (A through D) are the SEM micrographs of the bare SPIO, HP-SPIO, DOX- HP-SPIO and PTX- HP-SPIO NPs, respectively. (E) In vitro drug loading behavior of DOX and PTX from DOX-HP-SPIO and PTX-HP-SPIO NPs at pH 7.4.

10 **Figure 5A** demonstrates the schematic cutaway of drug-loaded (DOX or PTX), HP-coated Fe<sub>3</sub>O<sub>4</sub> nanoparticles. **Figure 5B** demonstrates the UV-Vis spectra of bare (492 and 529 nm), HP-SPIO (223 nm), pure DOX (486 nm), DOX-HP-SPIO NPs (320 and 507 nm), pure PTX (234 nm) and PTX-HP-SPIO-NPs (266 and 492 nm).

To confirm drug loading onto HP-SPIO NPs, FT-IR spectra of (a) bare SPIO NPs, (b) pure HP, (c) free DOX, (d) DOX-HP-SPIO, (e) free PTX and (f) PTX-HP-SPIO NPs were obtained (**Figure 5C**). SPIO NP spectrum showed 560 cm<sup>-1</sup> vibration

for Fe-O. HP spectrum showed  $3510\text{ cm}^{-1}$  ( $-\text{COO}^-$ )  $1774$  and  $1315\text{ cm}^{-1}$  ( $-\text{SO}_4^-$ ) vibrations. DOX spectra showed  $3340\text{ cm}^{-1}$  ( $\text{C}=\text{O}$  stretching),  $2870\text{ cm}^{-1}$  (asymmetric methylene group stretching),  $1730\text{ cm}^{-1}$  ( $\text{C}=\text{O}$  stretching),  $1690$ ,  $990$  and  $760\text{ cm}^{-1}$  ( $\text{O}-\text{H}$  out-of-plane bending). While, DOX-HP-SPIO NPs spectra showed  $3650\text{ cm}^{-1}$  ( $\text{O}-\text{H}$  stretching),  $2859$  (asymmetric methylene group stretching),  $1610\text{ cm}^{-1}$  ( $\text{C}=\text{O}$  stretching),  $1596\text{ cm}^{-1}$  ( $\text{O}-\text{H}$  bending) and  $790\text{ cm}^{-1}$  ( $\text{Fe}-\text{O}$  stretching). PTX spectra of  $1350$ ,  $1087$  and  $710\text{ cm}^{-1}$  were related to  $\text{CH}_3$  deformation,  $\text{C}-\text{O}$  stretching and  $\text{C}-\text{C}=\text{O}$  deformation. While  $3567\text{ cm}^{-1}$  in PTX-HP-SPIO NPs spectra were related to  $\text{N}-\text{H}/\text{O}-\text{H}$  stretching,  $1495\text{ cm}^{-1}$  for  $\text{CH}_3$  deformation,  $890\text{ cm}^{-1}$  for  $\text{C}-\text{H}$  in-plane deformation and  $450\text{ cm}^{-1}$  for  $\text{Fe}-\text{O}$  stretching. for Results show that the hydrophobic drugs like PTX and DOX were partitioned in the iron oxide core of HP-SPIO NPs. This method has the advantage of offering greater flexibility of loading the hydrophobic drugs.

10

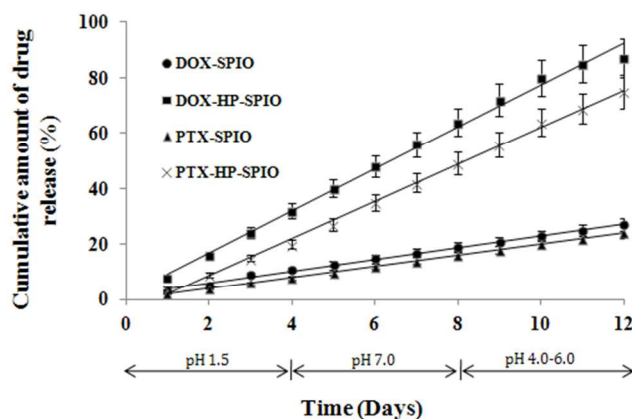


15

**Figure 5.** (A) Schematic cutaway of drug-loaded (DOX or PTX), HP-coated  $\text{Fe}_3\text{O}_4$  nanoparticles. (B) UV-Vis spectra of bare, HP-coated and drug (DOX and PTX) loaded SPIO-NPs. (C) FT-IR spectra of bare SPIO NPs, pure HP, free DOX, DOX-HP-SPIO NPs, free PTX and PTX-HP-SPIO NPs.

### 20 3.3. Drug release profile

The release study was carried out to estimate the amount of drug releasing from the HP-SPIO NPs under in vitro conditions. According to **Figure 6**, the release of free and combined DOX and PTX was 26, 87, 24 and 75%, respectively. Both individual and combined drug formulations showed sustained release of drug up to more than 15 days. The diffusion of anticancer drugs loaded into the polymeric shell could be due to the influence of concentration gradient, which is similar to the observations in oleic acid coated iron oxide nanoparticles (Jain et al., 2005). Thus, our formulation offered sustained release of anticancer drugs from the HP-SPIO NPs, which is an essential requirement for cancer therapy.



10

**Figure 6.** (F) In vitro release profiles of DOX and PTX from HP-SPIO NPs at pH 1.5-7.0, at 37 °C (n = 3).

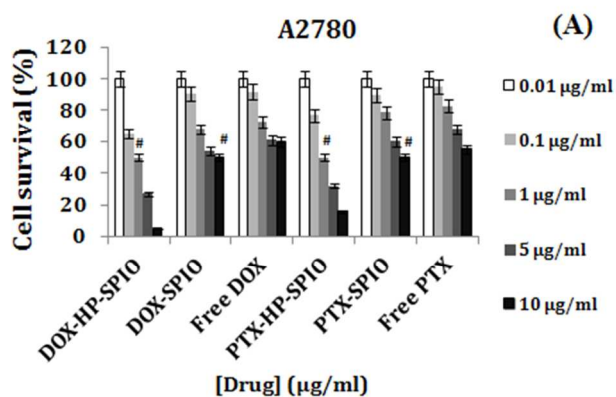
**Figure 6** shows the DOX release profiles of the free and conjugated DOX and PTX at the pH range of 1.5 - 7.0. At pH 7.0, a small amount of the drug release was observed after the incubation period of 48 hours. This is a desirable characteristic as the pH 7.4 is the undesired pH for the proper release of drugs from nano-conjugated drug carrier. This will also prevent the premature release of the drugs before the nano-conjugates reach the cancer cells. **Figure 6** shows that the pH 6.0 provided the desirable conditions for the proper drug release. The first 10 hours represent the period of initial rapid release, followed by a steady state. This pH-dependent drug release behavior is favorable for the chemotherapeutic process as it can significantly reduce the pre-term drug release at the body pH level (pH 7.4) and maximizing the amount of drug reaching the target tumor cells, once the drug-loaded nano-composites internalize and enter the tumor by endocytosis (pH 4.5-6.5).

### 3.4. Cellular cytotoxicity followed by uptake of drug loaded HP-SPIO NPs

For MTT assay, A2780 and OVCAR-3 cells were separately incubated with 0.1-10  $\mu\text{g/ml}$  DOX and PTX for 48 hours. According to **Figures 7A and B**, 10  $\mu\text{g/ml}$  of either DOX or PTX were the most effective against A2780 (60 and 55% survival) and OVCAR-3 cells (69 and 57% survival), respectively ( $p < 0.01$ ). So, this drug concentration was used for further experiments. While, 5 and 16% survival was seen in A2780 cells and, 15 and 50% in OVCAR-3 cells when incubated with DOX-HP-SPIO NPs and PTX-HP-SPIO NPs for 48 h, respectively.

As shown by the (#) marks in the plots of **Figures 7A and B**, the  $\text{IC}_{50}$  analysis revealed that 1  $\mu\text{g/ml}$  concentration of the DOX and PTX drugs, loaded in HP-SPIO NPs was the dose at which 50% of the A2780-cell growth was inhibited. The same pattern was seen in the OVCAR-3 cells, treated with DOX-HP-SPIO NPs. While, 5  $\mu\text{g/ml}$  concentration of PTX, loaded in HP-SPIO, was the  $\text{IC}_{50}$  against OVCAR-3 cell growth ( $p \leq 0.5$ ). In addition, 10  $\mu\text{g/ml}$  concentration of the DOX and PTX, loaded in bare SPIO NPs was recorded to be the  $\text{IC}_{50}$  against both cell lines, as compared to the control group (data not shown because of being non-significant) ( $p < 0.01$ ). This drug concentration was 10 times more than that delivered by the HP-SPIO NPs ( $p < 0.01$ ). This is important to state that free drugs could not receive to the  $\text{IC}_{50}$  values at the experimental concentrations of 0.1-10  $\mu\text{g/ml}$ . These results prove the significance of heparin coating onto the SPIO NPs and targeting the A2780 and OVCAR-3 cells with much lower concentrations of DOX and PTX, loaded in these novel nanocomposites.

**Figures 7 (C-F)** show the confocal fluorescence micrographs of A2780 (C & D) and OVCAR-3 cells (E & F), incubated for 3 h with DOX-HP-SPIO NPs and PTX-HP-SPIO NPs, labeled with FITC. In addition, about 50% survival was observed in A2780 and OVCAR-3 cells when treated with DOX-SPIO NPs and PTX-SPIO NPs, respectively ( $p < 0.05$ ). While, 43% survival was seen in A2780 cells when administered with PTX-SPIO NPs.



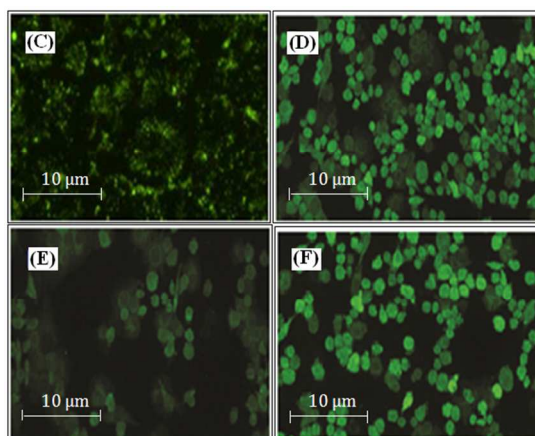
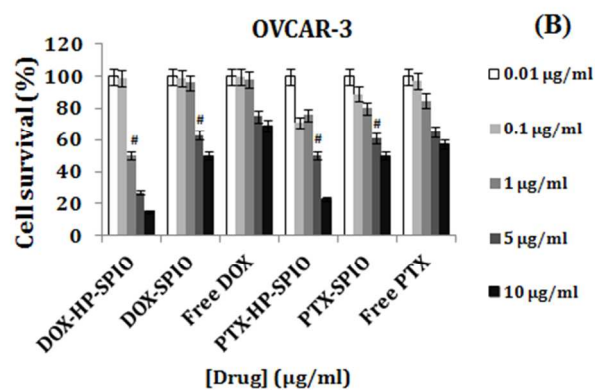


**Figure 7.** Results of the MTT assay for the determination of % viability in (A) A2780 and (B) OVCAR-3 human ovarian cancer cells, incubated for 48 hours with 0.1-10 µg/ml DOX, PTX, DOX-SPIO, PTX-SPIO, DOX-HP\_SPIO and PTX-HP-SPIO NPs<sup>10</sup>. Confocal fluorescence micrographs of A2780 (C & D) and OVCAR-3 cells (E & F), incubated for 3 h with DOX-HP-SPIO NPs and PTX-HP-SPIO NPs, labeled with FITC.

### 3.5. Apoptotic detection

10

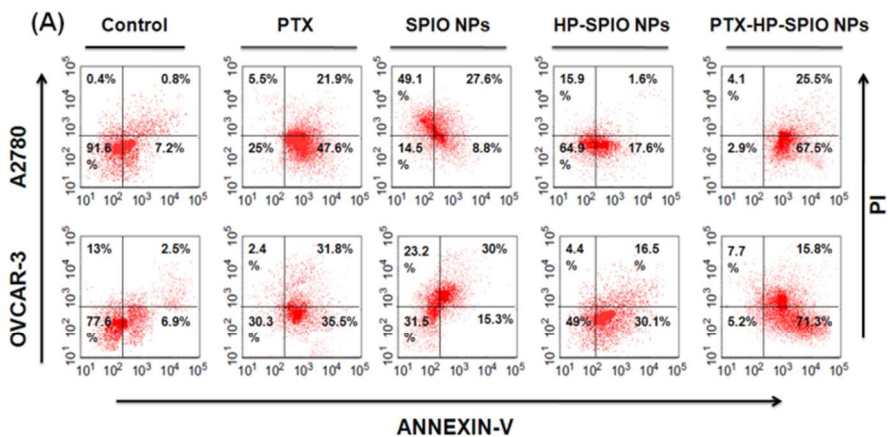
To compare the apoptotic activity of bare and drug loaded SPIO NPs, A2780 and OVCAR-3 cells were separately treated with fresh medium containing 10 µg/ml bare, HP-SPIO, DOX-HP-SPIO and PTX-HP-SPIO NPs for 48 hours. As shown in **Figure 8A**, A2780 and OVCAR-3 cells underwent 93 and 87.1% apoptosis, when administered with 5 µg/ml PTX-HP-SPIO NPs ( $p < 0.05$ ), as compared to the drug itself (69.5 and 67.3%, respectively). According to **Figure 8B**, DOX-HP-SPIO NPs caused 96.5 and 91.3% cell death in A2780 and OVCAR-3 cells, respectively, as compared to the DOX itself (70.9 and 62.7%;  $p < 0.05$ ).

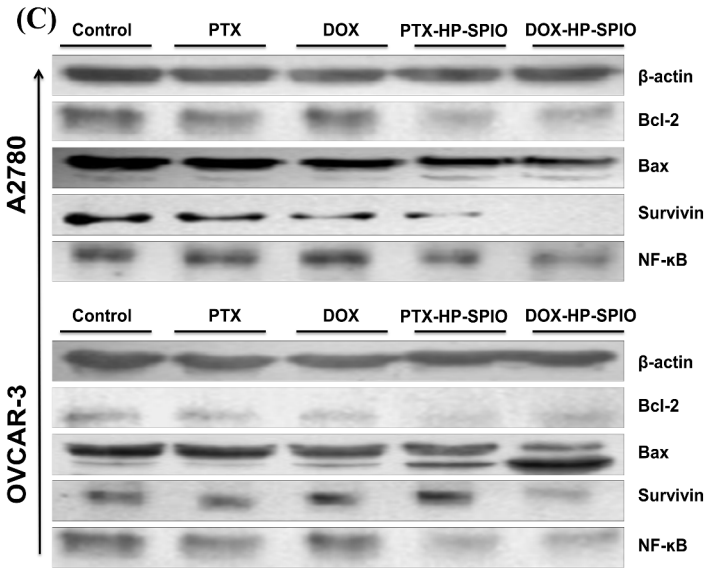
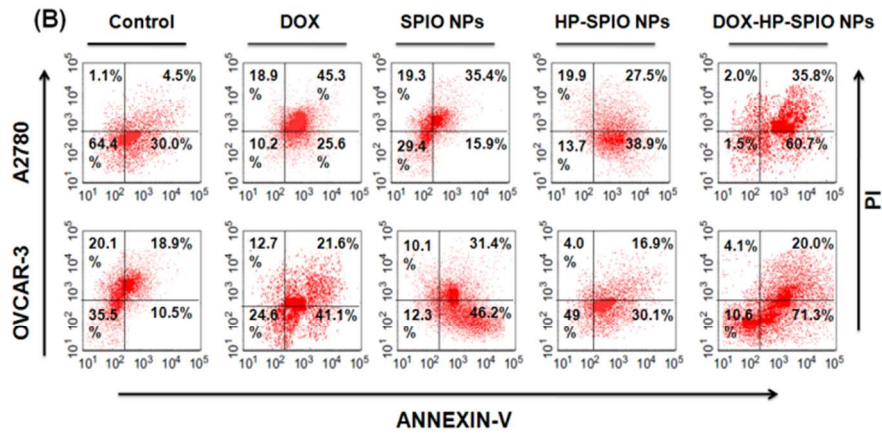
### 3.6. Western blot analysis for gene expression

During the present study, the expression of bax, bcl-2, NF- $\kappa$ B and survivin proteins were evaluated in A2780 and OVCAR-3 cells, treated with DOX, PTX, DOX-HP-SPIO NPs and PTX-HP-SPIO NPs, respectively. According to **Figure 8C**, the level of bcl-2 and survivin proteins had a sharp decrease while NF- $\kappa$ B was also regulated in the cultures, treated with DOX-HP-SPIO NPs in A2780 and OVCAR-3 cells. This represents the activation of apoptotic mechanism in cancer cells after the nanoparticle-based drug delivery in vitro ( $p < 0.05$ ).

### 3.7. Assessment of cell morphology

Figure 8D shows the bright-field phase contrast photographs of A2780 and OVCAR-3 cells, seeded with (10  $\mu$ g/ml drug) free PTX, free DOX, DOX-HP-SPIO and PTX-HP-SPIO NPs for 48 hours. The incubation of the cells with free drugs did not alter the morphology of A2780 and OVCAR-3 cell types. The viability of the cells after each period of incubation with the free DOX and PTX were close to that of the control cells and varied in the range from 92% to 96%, whereas DOX-HP-SPIO as well as PTX-HP-SPIO NPs were reported to have in vitro toxicity both cell lines, as shown by arrows. Both the particle size and material composition might play an important role in enhancing the cytotoxicity of nanocomposite-based drugs.





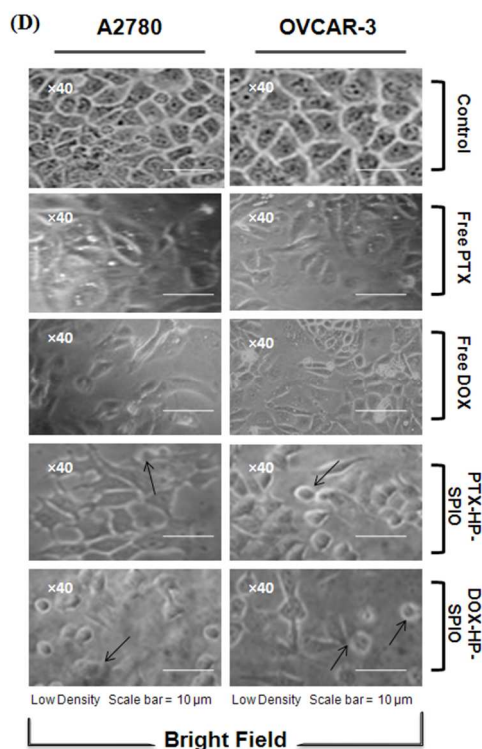


**Figure 8.** PTX (A) and DOX (B) loaded HP-SPIO NP system induces apoptosis in A2780 and OVCAR-3 cells. Both cancer cell lines were treated separately with DOX, PTX, SPIO NPs, HP-SPIO-NPs, DOX-HP-SPIO NPs and PTX-HP-SPIO NPs for 24 h. Apoptotic cell death was detected by staining the cells with Annexin V-FITC and propidium iodide (PI), and analyzed by flow cytometer. (C) Western analysis of the effects of free and nano-conjugated DOX and PTX on the expression of survivin, NF- $\kappa$ B, bcl-2 and bax in A2780 and OVCAR-3 cells. The cancer cells were incubated with 10  $\mu$ g/ml of DOX, PTX, DOX-HP-SPIO NPs and PTX-HP-SPIO NPs for 24h. As a control for loading, the blots were incubated with  $\beta$ -actin antibody. (D) Bright-field phase contrast photographs of A2780 and OVCAR-3 cells, administered with (10  $\mu$ g/ml drug) free PTX, free DOX, DOX-AP-SPIO and PTX-AP-SPIO NPs for 48 hours.

The intratumoral administration of anticancer drugs represents a growing trend for maximizing local tumor control with minimal systemic toxicity. However, it requires a novel drug delivery system for treatment efficacy and ease of administration. SPIO NPs have been widely used in the delivery of chemotherapeutics, achieving promising results (Dilnawaza et al., 2010).

The authors propose that combining intratumoral administration with a magnetic nanocarrier in chemotherapy provides opportunities for treating cancers in a safe and effective manner. We fabricated a SPIO-NP drug delivery system for intratumoral administration that was comprised of magnetic  $\text{Fe}_3\text{O}_4$  core and a shell of biocompatible material, heparin, coated onto the nanoparticles by a single emulsion evaporation method. The DOX-HP-SPIO NPs showed high loading content and encapsulation efficiency, and they supported a sustained and steady drug release (Lee et al., 2012). *In vitro*, the DOX-HP-SPIO NPs were easily internalized into the tumor cells and induced significant amount of apoptosis.

Systemic chemotherapy against cancers such as ovarian, breast, prostate, lung, and gastrointestinal cancers can cause severe side effects because of the toxicity caused by the anticancer drugs on normal tissues. Moreover, the efficacy of anticancer drugs can be diminished because of rapid clearance from circulation and poor distribution to the target tumor (Chari, 2008; Murakami et al., 2010). An intratumoral injection of chemotherapeutic agents is potentially a more effective alternative to systemic administration, because direct delivery of anticancer drug to the target may improve the stability and efficacy of anticancer drugs. Such targeted delivery would be expected to provide a high local concentration of agents, reducing systemic drug levels and thereby decreasing the incidence of side effects compared with traditional treatments (Springate et al., 2008).

The size of the nanoparticles is a key parameter that determines its properties, application and fate. First, given that the smallest capillaries in the body are about 4  $\mu\text{m}$ , particles larger than 4  $\mu\text{m}$  will most likely become trapped in the lungs (Neuberger et al., 2005). Particles smaller than that will usually be eliminated by reticuloendothelial system (RES). After intravenous administration, particles larger than 200 nm are usually sequestered by the spleen, as a result of mechanical filtration (Gupta & Gupta, 2005). These particles are eventually removed by phagocytes, resulting in decreased blood circulation times. On the other hand, particles smaller than 10 nm are rapidly removed through extravasations and renal clearance (Choi et al., 2007). Particles ranging from 10 to 100 nm are optimal for systemic administration and demonstrate the most prolonged blood circulation times. The particles in this size range are small enough to both evade the RES and penetrate the very small capillaries within the body tissues, and therefore they may offer the most effective distribution in certain tissues. However, complete evasion of the RES does not seem feasible and unwanted migration to normal tissues in the body could cause toxic side effects (Chouly et al., 1996).

In this study, we synthesized SPIO NPs, coated with unfractionated heparin (UF-HP) with the mean diameter of 42 nm and investigated the effect of the biodegradable nanocomposite coating on the targeted and efficient delivery of DOX and PTX to A2780 and OVCAR-3 cells. After drug loading, these nanocomposites acquired the size of about 85nm (DOX-HP-SPIO NPs) and 71 nm (PTX-HP-SPIO NPs). Particularly, we compared the uptake efficiency of nano-conjugated drugs as compared to the bare drugs (Lee et al., 2012). The uptake of nano-conjugated drugs is known to be mediated by endocytosis or phagocytosis. Therefore, incubation of drug loaded HP-SPIO NPs is required, for longer than several hours, to improve drug-release efficiency. Previous studies have reported that the iron content, taken in by cells has a broad range dependence on the cell type, exposure time and culture methods (10-120 pg Fe/cell, depending on the tissue and tumor type) (Arbab et al., 2004; Javid et al., 2013). During the present study, targeting the A2780 and OVCAR-3 cells required relatively long incubation time (~48 h) but smaller drug and nanocomposite concentrations (10  $\mu\text{g/ml}$ ), which may be attributed to the target-specificity and natural polymer (HP) coating.

Heparin has also been found to be an inhibitor of the replication of human immunodeficiency virus, and also an inhibitor of angiogenesis and tumours growth (Dias et al., 2011). Previous studies showed that the coating of HP on the surface of biomaterials increased hydrophilicity, which resulted in facilitated cell attachment to the biomaterial surface. Consistently, heparin coating of SPIO increased hydrophilicity, which may have caused enhanced cellular uptake (Jung et al., 2011).

Heparin is a highly sulfated natural glycosaminoglycan and recent studies have revealed that HP strongly binds to various growth factors such as vascular endothelial growth factor (VEGF) and epidermal growth factor (EGF) through the interaction with its sulfate group (Lee et al., 2012). The tumor cells hyper-express the growth factor receptors. So, we can assume that the increased internalization of SPIO NPs can be increased by its attachment with HP, which interacts with the growth hormones, 5 attached to their receptors on the tumor cells-membrane, rendering an increased uptake of drug-loaded nanoparticles (Lee, 2011).

In the present study, the drug release rate from HP-SPIO NPs was higher at the acidic pH (pH 6.0) than at the neutral pH (pH 7.4), which may lead to increased accumulation of DOX and PTX in tumor cells and thereby adding therapeutic efficiency to the delivery system (Li et al., 2012). After delivery to the tumor site, the next important step is internalization into the tumor 10 cell. This is directly related to the cytotoxicity of the drug, because DOX and PTX only show their antitumor efficiency when they bind to DNA or inhibit microtubule disassembly. In this study, the authors found the DOX-HP-SPIO NPs and PTX-HP-SPIO NPs were readily taken up by A2780 and OVCAR-3 cells, with a higher rate of cellular uptake and of larger amount than free drug. The drug-loaded SPIO NPs can be transported into tumor cells by a process called endocytosis or phagocytosis, through either specific or nonspecific cellular uptake, depending on the surface properties of the SPIO NPs (Huang et al., 15 2010). However, the exact mechanism of cellular uptake may be far more complicated than the current understanding, and further studies are clearly needed.

*In vitro*, the nanocomposite-based DOX and PTX were found to show a higher apoptosis-inducing effect in both cell lines than free drugs. These results are in agreement with previous reports. Kohler et al., (2006) reported that the methotrexate-immobilized poly(ethylene glycol) SPIO NPs induce higher cytotoxicity in glioma cells than free methotrexate, depending on 20 higher uptake and retaining its crystal structure in the cell cytoplasm. Chen et al., (2009) reported that the application of 5-bromotetrandrine and SPIO-NPs inhibited the expression of bcl-2 protein and upregulated the expression of bax and caspase-3 proteins in human leukemia K562 cells. These results are in line with our western blot and apoptosis analyses. The present results reveal that the SPIO NPs may suppress tumor cell proliferation and induce apoptosis by blocking multiple pathways.

#### 25 4. Conclusions

In summary, we constructed drug-loaded HP-SPIO NPs by a co-precipitation technique for intratumoral drug delivery. The nanoparticles supported sustained and steady release of DOX and PTX. Moreover, drug release from the HP-SPIO NPs was pH sensitive, with a faster release rate in an acidic environment than in a neutral environment. *In vitro*, the DOX-HP-SPIO NPs were readily internalized into tumor cells, and they induced a higher apoptosis rate. The heparin coating on nanoparticle 30 surface and its use in targeted drug delivery was demonstrated to increase the amount of NP uptake into ovarian cancer cells along with dramatic anti-noplastic activity, in comparison to free drugs. This suggests that the modification of SPIO NPs with HP could be used to formulate a better drug delivery vehicle and simultaneously facilitate the drug uptake to specific cancer

cells for successful cancer therapy. This work provides an exciting new modality for developing an effective drug delivery system.

## Acknowledgments

5

The authors are thankful to the Research Council of the University of Tehran, Tehran, Iran, for its financial support to the present work.

## References

- 10 S. Acharya, S.K. Sahoo, *Advanced Drug Delivery Reviews*, 2011, **63**, 170.
- A.S. Arbab, G.T. Yocum, H. Kalish, E.K. Jordan, S.A. Anderson, A.Y. Khakoo, *Blood*, 2004, **104**, 1217.
- H. Basti, L.B. Tahar, L.S. Smiri, F. Herbst, M. Vaulay, F. Chau, S. Ammara, S. Benderbous, *Journal of Colloid and Interface Science*, 2010, **341**, 248.
- R.V. Chari, *Accounts of Chemical Research*, 2008, **41**, 98.
- B. Chen, J. Cheng, Y. Wu, *International Journal of Nanomedicine*, 2009, **4**, 73.
- 15 H.S. Choi, W. Liu, P. Misra, *Nature Biotechnology*, 2007, **25**, 1165.
- C. Chouly, D. Pouliquen, I. Lucet, J.J. Jeune, P. Jallet, *Journal of Microencapsulation*, 1996, **13**, 245.
- A.M.C.G. Dias, A. Hussain, A.S. Marcos, A.S.A. Roque, *Biotechnology Advances*, 2011, **29**, 142.
- F. Dilnawaz, A. Singh, C. Mohanty, S.K. Sahoo, *Biomaterials*, 2010, **31**, 3694.
- L. Douziefch-Eyrolles, H. Marchais, K. Herve, *International Journal of Nanomedicine*, 2007, **2**, 541.
- 20 M.W. Freeman, A. Arrott, J.H.L. Watson, *Journal of Applied Physics*, 1960, **31**, S404.
- A.K. Gupta, M. Gupta, *Biomaterials*, 2005, **26**, 3995.
- X. Huang, X. Teng, D. Chen, F. Tang, J. He, *Biomaterials*, 2010, **31**, 438.
- T.K. Jain, M.A. Morales, S.K. Sahoo, D.L. Leslie-Pelecky, V. Labhasetwar, *Molecular Pharmacology*, 2005, **2**, 194.
- A. Javid, S. Ahmadian, A.A. Saboury, S.M. Kalantar, S. Rezaei-Zarchi, *Chemical Biology and Drug Design*, 2013, **82**, 296.
- 25 M.J. Jung, S.S. Lee, Y.H. Hwang, H.S. Jung, J.W. Hwang, M.J. Kim, S. Yoon, D.Y. Lee, *Biomaterials*, 2011, **32**, 9391.
- M.M. Kemp, R.J. Linhardt, *WIREs Nanomedicine and Nanobiotechnology*, 2010, **2**, 77.
- D.H. Kim, K.N. Kim, K.M. Kim, Y.K. Lee, *Journal of Biomedical Materials Research Part A*, 2009, **88A**, 1.
- N. Kohler, C. Sun, A. Fichtenholtz, J. Gunn, C. Fang, M. Zhang, *Small*, 2006, **2**, 785.
- S.J. Kyoung, D.P. Hyung, D.P. Ki, H.K. Young, S. Jung-Wong, *Biomacromolecules*, 2004, **5**, 1877.
- 30 D. Lee, *Macromolecular Research*, 2011, **19**, 843.
- J. Lee, M. Jin Jung, Y.H. Hwang, Y.J. Lee, D.S. Lee, D.Y. Lee, H. Shin, *Biomaterials*, 2012, **33**, 4861.
- A. Li, J.K. Kim, K.M. Huh, Y. Lee, S.Y. Kim, *Carbohydrate Polymers*, 2012, **87**, 2120.
- X. Liu, M.D. Kaminski, Y. Guan, H. Chen, H. Liu, A.J. Rosengart, *Journal of Magnetism and Magnetic Materials*, 2006, **306**, 248.
- M. Mahmoudi, S. Sant, B. Wang, S. Laurent, T. Sen, *Advanced Drug Delivery Reviews*, 2011, **63**, 24.
- 35 N. Meng, S. Zhang, N. Zhou, J. Shen, *Nanotechnology*, 2010, **21**, 185.
- T. Murakami, K. Tsuchida, M. Hashida, H. Imahori, *Molecular Biosystems*, 2010, **6**, 789.
- T. Neuberger, B. Schopf, H. Hofmann, M. Hofmann, B. von Rechenberg, *Journal of Magnetism and Magnetic Materials*, 2005, **293**, 48.
- S.K. Sahoo, V. Labhasetwar, *Drug Discovery Today*, 2003, **8**, 1112.

- K.K. Sang, V. Bagalkot, L. Eunhye, L. Seulki, L. Yong-kyu, S.K. Tadiparthi, T.M. Hyun, Y. Byun, *Thrombosis Research*, 2006, **117**, 419.
- C.M. Springate, J.K. Jackson, M.E. Gleave, H.M. Burt, *International Journal of Pharmacology*, 2008, **350**, 53.
- E. Strable, J.W.M. Bulte, B. Moskowitz, K. Vivekanandan, M. Allen, T. Douglas, *Chemistry of Materials*, 2001, **13**, 2201.
- S.K. Sahu, S. Maiti, A. Pramanik, S.K. Ghosh, P. Pramanik, *Carbohydrate Polymers*, 2012, **87**, 2593.
- 5 M. Vandana, S. Sahoo, *Nanomedicine*, 2009, **4**, 773.
- A. Villanueva, M. Cañete, A.G. Roca, M. Calero, S. Veintemillas-Verdaguer, C.J. Serna, *Nanotechnology*, 2009, **20**, 1.
- X. Wang, Y. Wang, Z.G. Chen, D.M. Shin, *Cancer Research and Treatment*, 2009, **41**, 1.